LA-UR- 97-4004
CONF-9705230--

A COMPARISON BETWEEN THE IRRADIATION DAMAGE RESPONSE OF SPINEL AND ZIRCONIA DUE TO Xe ION BOMBARDMENT

Kurt E. Sickafus, Christopher J. Wetteland, Neil P. Baker, Ning Yu, Ram Devanathan, Michael Nastasi, and Nicole Bordes

Los Alamos National Laboratory, Division of Materials Science & Technology, Los Alamos, New Mexico, U.S.A.

Phone (505) 665-3457; Fax (505) 665-9224; E-mail: kurt@lanl.gov

ABSTRACT

The mechanical properties of Xe-implanted spinel and cubic zirconia surfaces, as determined by nano-indentation measurements, are distinct and the differences can be related to their microstructures. Upon Xe^{++} ion irradiation at cryogenic temperature (120K), the Young's modulus of irradiated spinel increases slightly (a few percent) then falls dramatically until the modulus is only about 3/4 the unirradiated value. The maximum modulus occurs concurrent with the formation of a metastable crystalline phase of spinel. The subsequent elastic softening at higher Xe^{++} doses is an indication of the onset of amorphization of the spinel. Xe-implanted zirconia surfaces behaves differently, in all cases showing almost no change in elastic modulus with increasing Xe^{++} ion dose. This is consistent with microstructural observations of Xe-implanted zirconia crystals which, unlike spinel, show no change in crystal structure with increasing ion dose. The defected layer in zirconia due to ion damage simply thickens with increasing Xe^{++} dose. This thickening may be a consequence of compressive stresses that form in the ion-implanted surface region. The hardness of both spinel and zirconia increases slightly for low Xe^{++} ion doses. At higher doses, zirconia shows little change in hardness, while the hardness of the implanted spinel falls by more than a factor of two. The initial increase in hardness of both spinel and zirconia is probably due to point defect accumulation and the precipitation of small interstitial clusters, while the drop in hardness of spinel at high Xe^{++} ion doses is due to the formation of an amorphous phase.

Introduction

The oxides magnesio aluminate spinel ($MgAl_2O_4$) and cubic-stabilized zirconia (ZrO_2-Y_2O_3) have been demonstrated to exhibit exceptional radiation tolerance, both under fast neutron irradiation [1, 2] and ion irradiation [3, 4]. Nevertheless, heavy ion implanted spinel and zirconia display complicated implantation microstructures and altered surface mechanical properties [5]. Thus, it is interesting to compare the vastly different damage evolution in two ceramic oxides that are nominally radiation resistant.

Spinel implanted with 370-400 keV Xe ions resists amorphization at elevated temperature (670K) to a peak damage level of 50 displacements per atom (dpa) [6]. At cryogenic temperature (100K), an amorphous layer is formed at the sample surface at a peak damage level of 25 dpa [7]. It has been established that this amorphization of spinel is not entirely a chemical effect due to implanted Xe [8]. This was demonstrated by irradiating fragments of spinel with highly penetrating 1.5 MeV Xe^+ ions. In this case, the edges of the spinel crystallites were rendered amorphous at a dose of about 35 dpa for an irradiation temperature of 30K. In all of these samples, transmission electron microscopy (TEM) revealed that irradiated regions that remain crystalline are heavily defected and exhibit a crystal structure different than ordinary spinel. The new crystal structure in these regions is related to the disordering of cations and to displacement of cations into interstitial sites [9, 10]. Since the radiation damage response of spinel is strongly temperature-dependent, point defect mobility in spinel is apparently dictated by thermal activation mechanisms.

Cubic zirconia implanted with 400 keV Xe ions at cryogenic and ambient temperatures (180K and 300K, respectively) exhibits a very different irradiation damage response compared to spinel. No amorphization is observed in zirconia to a peak damage level of about 80 dpa [11]. Furthermore, the lattice disorder induced by implantation (determined from ion channeling measurements) saturates to the same level, irrespective of irradiation temperature [11]. TEM measurements indicate that several microstructural zones form along the Xe irradiation direction, including a heavily-defected layer beneath a defect-denuded zone at the surface [11]. With increasing dose, the heavily-defected layer penetrates well beyond the projected range of the Xe ions (75 nm) to a depth of ~160 nm at the maximum experimental fluence ($3 \cdot 10^{20}$ Xe^{++}/m^2). These observations indicate that radiation-induced point defects in zirconia are highly mobile, even under cryogenic irradiation conditions.

In this paper, we investigate the mechanical properties of Xe-implanted spinel and cubic-stabilized zirconia surfaces. We measure elastic (Young's) modulus, E, and hardness, H,

using the nano-indentation technique. Mechanical property changes as a function of Xe^{++} ion dose are compared to microstructural observations on similarly implanted samples.

Experimental Procedure

Synthetic single crystals of 'stoichiometric' $MgO{\bullet}Al_2O_3$ ($MgAl_2O_4$) spinel with (001) orientations were used for this study (crystals were originally obtained from Linde Division, Union Carbide Corp.). The zirconia crystals used in this study were (001)-oriented cubic zirconium dioxide (ZrO_2) substrates stabilized with 9.5 mole % Y_2O_3 (the equivalent composition is given by $Zr_{0.8265}Y_{0.1735}O_{1.913}$). These crystals were obtained from Zirmat Corp. (P.O. Box 365, N. Billerca, MA 01862). Both spinel and zirconia crystal substrates were cut to dimensions of approximately 10mm x 10mm x 0.5mm and polished on one side to a mirror finish.

Samples were irradiated with 370 keV Xe^{++} ions using a 200 kV ion implanter in the Ion Beam Materials Laboratory (IBML) at Los Alamos National Laboratory (LANL). The samples were tilted to about 15° with respect to the incident ion beam, in order to minimize ion channeling effects during the irradiations. Ion doses ranged from $5{\bullet}10^{18}$ - $1{\bullet}10^{20}$ Xe/m^2. The sample stage was cooled to a temperature of about 120K by liquid nitrogen conduction cooling. Temperature excursions during irradiations were about ±5K, as measured using a thermocouple attached to the sample stage. The Xe^{++} ion flux was maintained at between 3 - 6 $\bullet 10^{17}$ $Xe^{++}/m^2{\bullet}s$, corresponding to a peak damage rate of about 0.1 dpa per second. Spinel and zirconia substrates were irradiated simultaneously in each irradiation experiment. The specific Xe^{++} ion doses used in this experiment, in units of Xe/m^2, were: (a) $5{\bullet}10^{18}$; (b) $1.0{\bullet}10^{19}$; (c) $1.5{\bullet}10^{19}$; (d) $1.75{\bullet}10^{19}$; (e) $2.5{\bullet}10^{19}$; (f) $3{\bullet}10^{19}$; (g)$5{\bullet}10^{19}$; (h) $1{\bullet}10^{20}$. One unirradiated substrate of spinel and one of zirconia were used as control samples.

Nano-indentation was used to investigate the mechanical properties of unirradiated and irradiated spinel and zirconia samples. This technique uses indentation load-displacement behavior to assess the near-surface mechanical properties of materials, such as elastic modulus, E, and hardness, H. In these experiments, a Nano Indenter® II instrument (Nano-indenter is a registered trademark of Nano Instruments, Inc., P.O. Box 14211 Knoxville, TN 37914) was used for the load-displacement measurements. For these measurements, a Berkovich indenter (a three-sided pyramidal diamond with an area-to-depth function equivalent to a Vickers indenter) was used. Also, the measurements of E and H were made using the continuous stiffness method (CSM), a dynamic method

wherein load and displacement are continuously increased and monitored in each indentation test [12]. This is accomplished by applying a small amplitude, high-frequency (69.3 Hz) oscillation to the force signal. The corresponding displacement oscillation is monitored using phase-sensitive detection (a lock-in amplifier) at the excitation frequency. These were displacement-controlled experiments, in the sense that load-displacement measurements were obtained at pre-programmed displacement intervals of about 5 nm and the indentation process was terminated at a maximum displacement of about 100 nm. The load range for these experiments was approximately 0 - 4 mN. Each sample was subjected to ten indentation (continuous stiffness, load-displacement) measurements. Indents were placed approximately 15 μm apart in a 5x2 rectangle. A fused silica sample was used as a control and tested at the outset of each experiment. The fused silica is also the calibration standard for the determination of H, which is given by the load at a given indenter displacement divided by the contact area of the indenter at that displacement. E is determined from the slope of the force-displacement unloading curve. Though the samples were all single crystals, the measured modulus is expressed simply as E, since the indenter produces displacements and plastic flow in many directions. Under these conditions, the measured modulus is best represented as an average of the elastic constants, e.g. a Voigt-Reuss-Hill average [13]. A detailed discussion of the determination of H and E from load-displacement curves for loading and unloading may be found in References [14] and [12].

Nano-indentation, formerly called ultramicrohardness, is particularly useful compared to conventional micro-indentation for the measurement of mechanical properties of implanted surfaces, because the sample is only deformed to depths of the order of several nanometers (e.g., see [15]). A guiding rule is that indentation depths should not exceed 10-25% of the thickness of the surface layer to be probed [14], so as to minimize the influence of the substrate on the measured mechanical properties. In the ion-implanted samples used for this study, the surface layer modified by irradiation is expected to be less than 200 nm thick. So, for the smallest displacements available by the nano-indentation technique, the mechanical properties of the irradiated layer may be probed without significant influence from the unirradiated substrate, while at the maximum indentation depth (~100 nm) substrate influence is expected to be observable.

The projected range of 370 keV Xe^{++} ions and the number of atomic displacements produced per ion in spinel and zirconia were estimated from Monte Carlo simulations using the TRIM binary collision code [16] (specifically, using SRIM, i.e., TRIM-96). Results of these simulations are shown in Figure 1. For the calculations shown in Fig. 1, we used a density of 3.58 g/cm^3 for stoichiometric spinel (JCPDS file 21-1152 [17]) and 5.959 g/cm^3

for yttria-cubic-stabilized zirconia (from JCPDS file 30-1468 [17], for composition $Zr_{0.85}Y_{0.15}O_{1.93}$, close to the composition of our samples), and a threshold displacement energy of 40 eV for all elements. In spinel, the range of 370 keV Xe^{++} ions is ~95 nm and the longitudinal straggling of the ions is ~22 nm. In zirconia, the range of 370 keV Xe^{++} ions is ~77 nm and the longitudinal straggling of the ions is ~27 nm. The peak concentration of Xe per 10^{20} Xe/m^2 dose, in the irradiated spinel and zirconia is about 1.7 at.% and 1.85 at.%, respectively. For the largest ion dose used in this study, $1 \cdot 10^{20}$ Xe/m^2, TRIM simulations indicate that the peak damage level (averaged over cation and anion sublattices) is about 28 dpa for spinel and 34 dpa for zirconia. The depths at which we expect to observe the peak concentrations of Xe in our experiments should be about 4% less than those indicated in these TRIM calculations, due to the 15° tilt of the substrate relative to the ion beam (tilt employed to avoid ion channeling effects); likewise for the peak displacement damage depths.

Results & Discussion

Figure 2 shows a plot of the elastic (Young's) modulus, E, as a function of indenter displacement for unirradiated spinel (Fig. 2a) and unirradiated zirconia (Fig. 2b). The error bars represent the scatter in the data obtained for the modulus at each indenter displacement interval for 10 separate indentations. For both spinel and zirconia, E is observed to rise with increasing displacement, then saturate to a constant value, nearly independent of displacement.[1] The modulus values for both spinel and zirconia saturate at about 280 GPa. The spinel value of E is in good agreement with reported values of the room temperature, elastic modulus of spinel [18]. The reported value of the Young's modulus at 293K of cubic-stabilized zirconia containing 11.1 mole % Y_2O_3 (equivalent to $Zr_{0.8002}Y_{0.1998}O_{1.900}$, a

[1] For this study, we also prepared spinel and zirconia crystal substrates that we chemically etched in boiling orthophosphoric acid for 20 - 30 minutes. We did this in an effort to remove the residual surface damage associated with mechanical polishing. The load-displacement results obtained from these etched samples of spinel and zirconia were not nearly so well-behaved as the unetched samples and in fact, could not be used to interpret modulus and hardness changes due to ion implantation. We presume that the poor indentation behavior of the etched substrates was due to excessive surface roughness induced by our chemical etch treatment. However, in related experiments in which we used Rutherford backscattering and ion channeling to measure radiation damage accumulation in these samples, we found that the etched crystals were superior to polished crystals for ion channeling measurements. The etching process removes some of the near-surface damage due to polishing and this improves the ion channeling behavior of the crystals. Nevertheless, the only indentation data presented here will be results from polished, unetched crystals.

slightly higher concentration of Y_2O_3 than in our crystals) is 228 GPa [19], about 18% lower than our measured value. We do not have an explanation for this discrepancy.

Figure 3 shows Young's modulus versus indenter displacement for spinel (Fig. 3a) and zirconia (Fig. 3b) crystals, irradiated to a Xe^{++} ion fluence of $2.5 \cdot 10^{19}$ Xe^{++}/m^2. Again, the moduli of both spinel and zirconia are observed to increase with increasing displacement. For zirconia, *E* saturates rapidly to a value similar to the saturated value for the unirradiated zirconia crystal. In irradiated spinel, *E* rises much more slowly with increasing indenter displacement, compared to the unirradiated crystal (Fig. 2a) and at the maximum displacement value of about 107 nm, *E* has not quite returned to the value of 280 GPa obtained for unirradiated spinel.

Figures 4, 5, and 6 show the variation of Young's modulus with Xe^{++} ion fluence at an indenter displacements of approximately 20 nm, 40 nm, and 80 nm, respectively. These plots are obtained using the measured *E* values at fixed indenter displacements, in load-displacement curves (such as those shown in Figs. 2 and 3) from all of the irradiated samples. The scatter in the data in Figs. 4-6 is greatest for the smallest indenter displacement (20 nm) and improves with increasing displacement. There is little change observed in *E* as a function of Xe^{++} ion fluence in the case of zirconia (Figs. 4b, 5b, and 6b). Spinel exhibits a small increase in *E* with increasing ion fluence (not apparent at 20 nm displacement, Fig. 4a; a 3% rise is observed at 80 nm displacement, Fig. 6a), followed by a dramatic fall in *E* for Xe^{++} ion fluences greater than about $1.75 \cdot 10^{19}$ Xe^{++}/m^2 (the decrease in E at 40 nm displacement is about 30%, Fig. 5a).

We have observed variations in *E* with Xe ion irradiation in spinel before [5, 20], and have demonstrated that the slight increase in *E* at low ion dose (equivalent to 3-5 dpa peak displacement damage) occurs commensurate with the formation of a metastable phase of spinel, while the substantial decrease in *E* for doses in excess of about 6 dpa (peak displacement damage) is indicative of an amorphization transformation. We observe here that the elastic modulus of zirconia is almost unchanged over the same range of ion fluences (to a maximum ion dose equivalent to about 34 dpa peak displacement damage). The changes in *E* observed in spinel are due to structural transformations, i.e., specific changes in the local and global arrangements of the atoms. In zirconia, we observed no such changes in structure due to Xe^{++} ion irradiation [11] and so it is not surprising that here, we find no evidence for changes in zirconia's modulus, *E*. In zirconia, we observed a high concentration of small (5-20 nm diameter) defect clusters in a crystal irradiated to a peak displacement damage level of ~80 dpa at 180K, but the crystal structure of the ion irradiated surface region was identical to the unirradiated substrate, as evidenced by electron

microdiffraction [11]. We conclude that since elastic modulus is an intrinsic property of a material, we should only expect to observe modulus changes when structural transformations are induced by irradiation. Two distinct transformations occur in spinel with increasing ion fluence and variations in E are observed accordingly, while no transformations are observed in zirconia; hence, in zirconia we observe a constant E versus ion dose dependence. Our understanding of the nature of the metastable phase produced in ion-irradiated spinel is detailed elsewhere [5, 20, 21]. We do not yet understand the reason for an increase in modulus upon formation of the metastable phase. The decrease in E upon amorphization is a lattice-softening effect, typical of amorphization transformations (e.g., an elastic softening of about 50% has been reported in Zr_3Al following radiation-induced amorphization [22]). It is interesting to note that in a related ion irradiation damage study of spinel in which we used much more highly penetrating 12 MeV Au^{3+} ions, we observed no phase transformations to 33 dpa peak displacement damage and likewise, we observed no change in Young's modulus [23]. This result conforms to our proposition here that E, as determined from nano-indentation measurements, is a good indicator for irradiation induced phase transformations in ion-implanted surfaces.

Figure 7 shows the measured variations in hardness, H, versus Xe^{++} ion dose, for both spinel and zirconia crystals. This data was obtained from load-displacement curves at an indenter displacement of about 62 nm. H for zirconia increases by about 5% to an ion fluence of $1 \cdot 10^{19}$ Xe^{++}/m^2, then remains constant with increasing ion dose. H for spinel increases initially by about 6% at a fluence of $5 \cdot 10^{18}$ Xe^{++}/m^2, then decreases sharply to less than half of its unirradiated value. In both spinel and zirconia, the increase in H at low Xe^{++} ion dose may be a hardening effect due to point defect accumulation, as well as to the precipitation of small defect clusters. The sharp decrease in H for Xe^{++} ion fluences greater than about $1.75 \cdot 10^{19}$ Xe^{++}/m^2 is due to the transformation to an amorphous phase and the lattice softening that accompanies this transformation. The fact that hardness is an extrinsic property, representing a material's ability to resist plastic deformation, explains why we observe changes in H in both spinel and zirconia. Though no radiation-induced crystal structure transformation is observed in zirconia, the accumulation of defects in the lattice can diminish its plasticity (due to mechanisms such as dislocation drag and dislocation pinning), and so enhances its hardness.

Figure 8 summarizes our comparison between the Xe^{++} ion irradiation damage response of spinel and zirconia single crystals. Fig. 8 shows schematic cross-sections of spinel and zirconia crystals subjected to increasing fluences of 370 keV Xe^{++} ions. Fluences of $5 \cdot 10^{18}$ Xe^{++}/m^2; $1.5 \cdot 10^{19}$ Xe^{++}/m^2; and $1 \cdot 10^{20}$ Xe^{++}/m^2 are illustrated in Fig. 8. At the

lowest ion fluence, representing a peak displacement damage of about 1.4 dpa in spinel and 1.7 dpa in zirconia, both oxides retain their original crystal structure (C), their elastic moduli are unchanged, and in each case, the hardness is increased slightly due to radiation-induced defect accumulation . A gradient in shading is shown in some of the crystal cross-sections in Fig. 8; this is intended to represent an increase in defect cluster concentrations with increasing depth. In earlier studies of both spinel [20] and zirconia [11], we have observed that the surface region is denuded of defect clusters, by comparison to the defect cluster concentrations observed at depths closer to the projected Xe^{++} ion range. By the intermediate ion fluence in Fig. 8, representing a peak displacement damage of about 4.2 dpa in spinel and 5.1 dpa in zirconia, spinel has transformed to a metastable crystalline phase (M), while the zirconia structure remains unchanged (C). E has increased slightly in spinel at this dose, but remains constant in zirconia, while H has saturated in zirconia and is beginning to fall in spinel. The ion damaged layers in both spinel and zirconia crystals are thicker than at the lower ion dose. We have evidence for this thickening both from ion channeling and electron microscopy studies [11, 20]. At the highest ion fluence in Fig. 8, representing a peak displacement damage of about 28 dpa in spinel and 34 dpa in zirconia, the spinel crystal has been rendered fully amorphous (A) by irradiation, while the structure of zirconia is identical to unirradiated zirconia (C). E and H are drastically reduced in the spinel crystal at this ion dose, but unchanged in zirconia, with respect to the values of E and H at the intermediate ion dose. In both spinel and zirconia, the irradiated layer thickness has increased further at this dose, reaching depths beyond the penetration of the Xe ions [11, 20], as well as beyond the depths associated with the displacement damage predicted by the TRIM simulations (Fig. 1). We believe these thickening effects are due to compressive stresses that arise in the implanted surfaces. These stresses encourage radiation-induced point defects to migrate into deeper, unirradiated material. These stresses can also influence other mechanical properties such as fracture toughness [11].

Conclusions

Surface mechanical properties of Xe^{++}-ion irradiated spinel and zirconia crystals were measured using the nano-indentation technique. The elastic (Young's) modulus, E, was found to be a sensitive indicator of radiation-induced phase transformations. In particular, E was found to increase in spinel upon formation of a metastable crystal phase (at doses equivalent to 3-5 dpa peak displacement damage) and then decrease sharply upon

transformation to an amorphous phase (at doses in excess of about 6 dpa peak displacement damage). On the other hand, E showed no significant variation in zirconia, to an ion dose equivalent to about 34 dpa peak displacement damage . Likewise, no structural phase transformations are observed in zirconia to this dose. The hardness, H, was observed to increase slightly (5-6%) in both spinel and zirconia at ion doses equivalent to about 1.5 and 3.5 dpa peak displacement damage, respectively. At higher doses, H is unchanged in zirconia, but falls dramatically in spinel upon formation of an amorphous phase. The initial rise in hardness in these oxides is probably due to the accumulation of radiation-induced point defects and the precipitation of small point defect clusters, while the subsequent decrease in H observed in spinel is due to the elastic softening that accompanies amorphization.

Acknowledgments

This research was sponsored by the US Department of Energy, Office of Basic Energy Sciences, Division of Materials Sciences.

References

[1] F. W. Clinard, Jr., G. F. Hurley and L. W. Hobbs, J. Nucl. Mater. **108/109** (1982) 655-670.

[2] F. W. Clinard, Jr., D. L. Rohr and W. A. Ranken, J. Am. Ceram. Soc. **60** (1977) 287-288.

[3] S. J. Zinkle, J. Am. Ceram. Soc. **72 (8)** (1989) 1343-1351.

[4] E. L. Fleischer, M. G. Norton, M. A. Zaleski, W. Hertl, C. B. Carter and J. W. Mayer, J. Mater. Res. **6** (1991) 1905.

[5] R. Devanathan, N. Yu, K. E. Sickafus and M. Nastasi, J. Nucl. Mater. **232** (1996) 59-64.

[6] N. Yu, K. E. Sickafus and M. Nastasi, Mater. Res. Soc. Symp. Proc. **373** (1995) 401-406.

[7] N. Yu, K. E. Sickafus and M. Nastasi, Phil. Mag. Lett. **70** (1994) 235-240.

[8] K. E. Sickafus, N. Yu and M. Nastasi, J. Nucl. Mater. (1997) in press (Los Alamos Report #LA-UR-96-1382).

[9] K. E. Sickafus, A. C. Larson, N. Yu, M. Nastasi, G. W. Hollenberg, F. A. Garner and R. C. Bradt, J. Nucl. Mater. **219** (1995) 128-134.

[10] R. Devanathan, N. Yu, K. E. Sickafus and M. Nastasi, Mater. Res. Soc. Symp. Proc. **398** (1996) 171-176.

[11] N. Yu, K. E. Sickafus, P. Kodali and M. Nastasi, J. Nucl. Mater. **244** (1997) 266-272.

[12] W. C. Oliver and G. M. Pharr, J. Mater. Res. **7** (1992) 1564-1583.

[13] R. Hill, Proc. Phys. Soc., London, Sect. A **65** (1952) 439-454.

[14] G. M. Pharr and W. C. Oliver, MRS Bull. **17** (1992) 28.

[15] J. B. Pethica, R. Hutchings and W. C. Oliver, Nucl. Instr. and Meth. **209/210** (1983) 995-1000.

[16] J. F. Ziegler, J. P. Biersack and U. Littmark, The Stopping and Range of Ions in Solids (Pergamon Press, New York, 1985).

[17] International Centre for Diffraction Data, Powder Diffraction File (Joint Committee on Powder Diffraction Standards, Philadelphia, PA, 1974 - present).

[18] A. Yoneda, J. Phys. Earth **38** (1990) 19.

[19] H. M. Kandil, J. D. Greiner and J. F. Smith, J. Am. Ceram. Soc. **67** (1984) 341-346.

[20] N. Yu, R. Devanathan, K. E. Sickafus and M. Nastasi, J. Mater. Res. **12** (1997) 1766-1770.

[21] R. Devanathan, N. Yu, K. E. Sickafus, M. Nastasi, M. Grimsditch and P. R. Okamoto, Phil. Mag. B **75** (1997) 793-801.

[22] L. E. Rehn, P. R. Okamoto, J. Pearson, R. Bhadra and M. Grimsditch, Phys. Rev. Lett. **59** (1987) 2987.

[23] R. Devanathan, N. Yu, K. E. Sickafus and M. Nastasi, Nucl. Instr. and Meth. B **127/128** (1997) 608-611.

Figure Captions

Figure 1. Calculated range of 370 keV Xe^{++} ions and the number of atomic displacements produced per Xe^{++} ion as a function of depth in (a) spinel and (b) zirconia, based on Monte Carlo simulations using the TRIM binary collision code. A threshold displacement energy of 40 eV was used for all elements.

Figure 2. Elastic (Young's) modulus, E, as a function of indenter displacement for (a) unirradiated spinel and (b) unirradiated zirconia.

Figure 3. Young's modulus E versus indenter displacement for (a) spinel irradiated to a Xe^{++} ion fluence of $2.5 \cdot 10^{19}$ Xe^{++}/m^2, and (b) zirconia irradiated to a Xe^{++} ion fluence of $2.5 \cdot 10^{19}$ Xe^{++}/m^2.

Figure 4. Young's modulus E versus Xe^{++} ion fluence at an indenter displacement of approximately 20 nm for (a) spinel crystals and (b) zirconia crystals.

Figure 5. Young's modulus E versus Xe^{++} ion fluence at an indenter displacement of approximately 40 nm for (a) spinel crystals and (b) zirconia crystals.

Figure 6. Young's modulus E versus Xe^{++} ion fluence at an indenter displacement of approximately 80 nm for (a) spinel crystals and (b) zirconia crystals.

Figure 7. Hardness, H, versus Xe^{++} ion dose for spinel and zirconia crystals. Data obtained from load-displacement curves at an indenter displacement of about 62 nm.

Figure 8. Schematic diagram showing cross-sections of spinel and zirconia crystals subjected to increasing fluences of 370 keV Xe^{++} ions. C stands for crystalline spinel or crystalline zirconia. M represents the metastable phase of spinel, and A represents the amorphous phase of spinel.

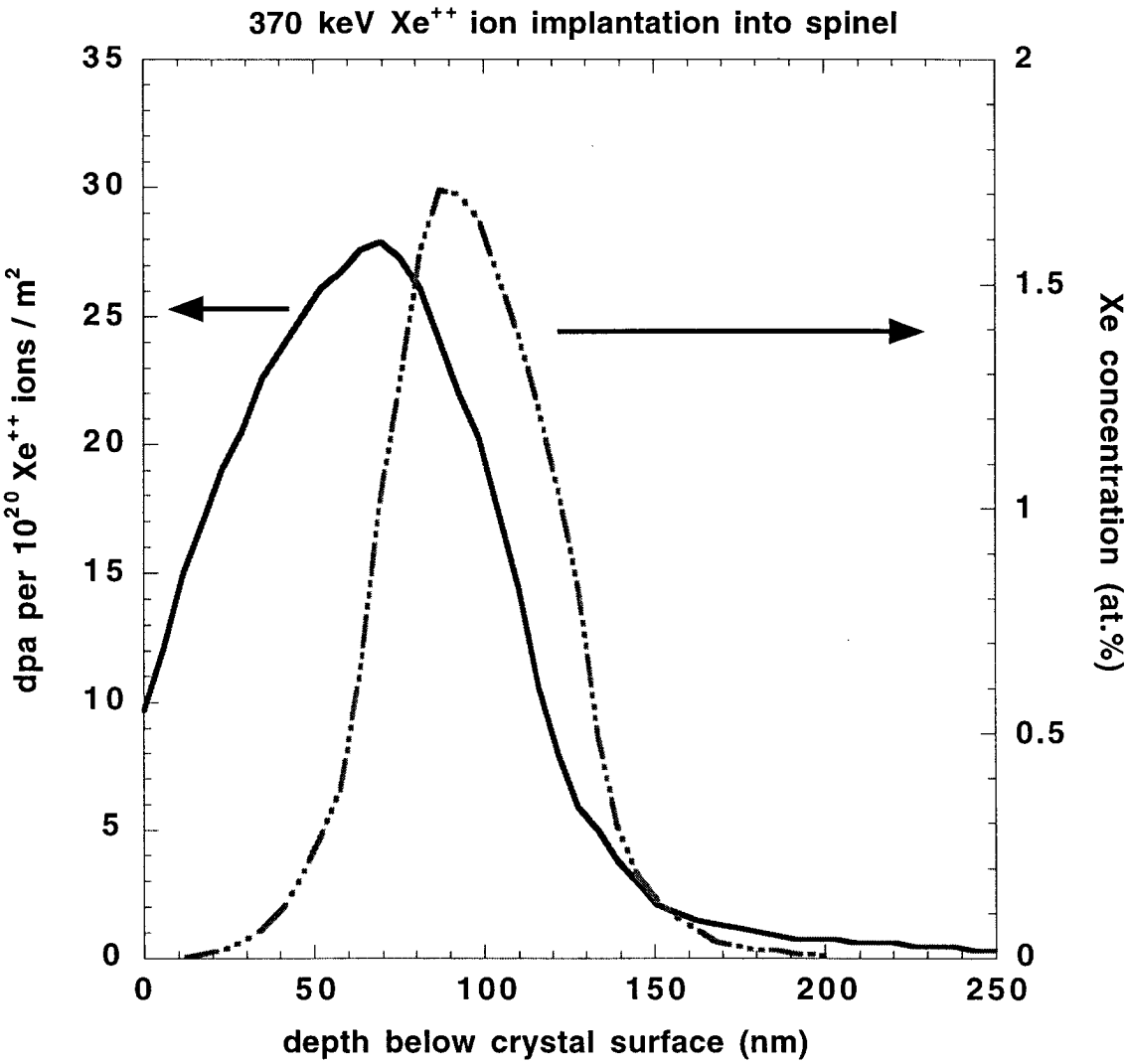
370 keV Xe++ ion implantation into spinel
dpa per 10^20 Xe++ ions / m^2
Xe concentration (at.%)
depth below crystal surface (nm)
0
5
10
15
20
25
30
35
0
0.5
1
1.5
2
0
50
100
150
200
250

Figure 1a

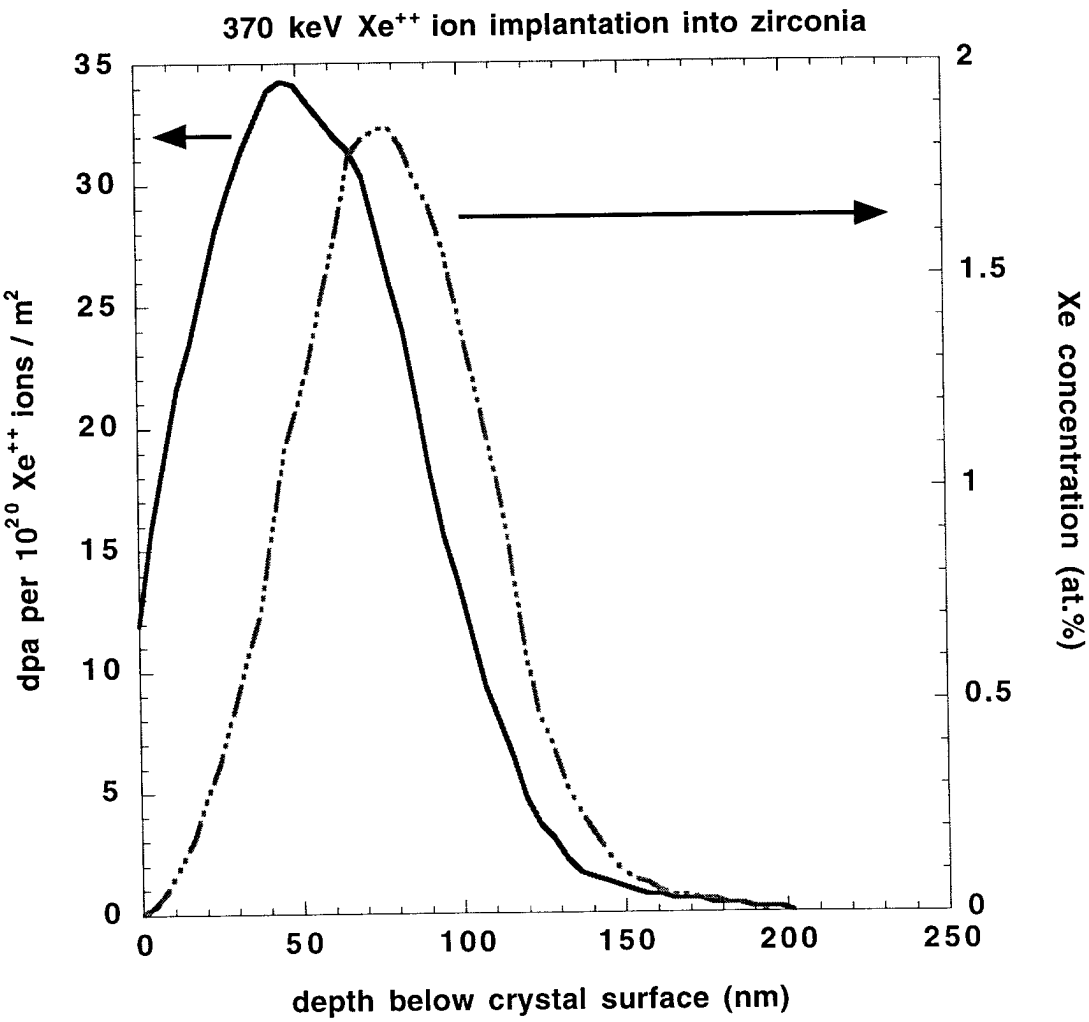
370 keV Xe++ ion implantation into zirconia
dpa per 10^20 Xe++ ions / m^2
Xe concentration (at.%)
depth below crystal surface (nm)
0
5
10
15
20
25
30
35
0
0.5
1
1.5
2
0
50
100
150
200
250

Figure 1b

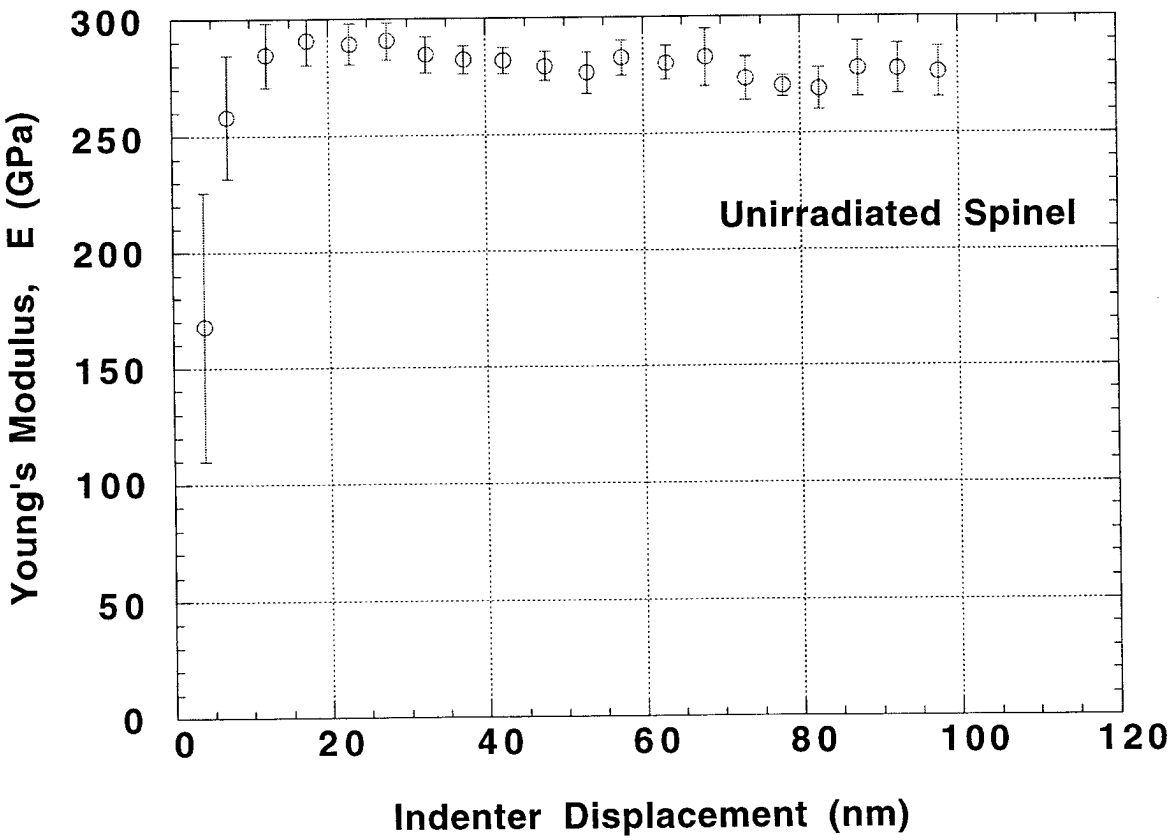
Young's Modulus, E (GPa)
300
250
200
150
100
50
0
0
20
40
60
80
100
120
Indenter Displacement (nm)
Unirradiated Spinel

Figure 2a

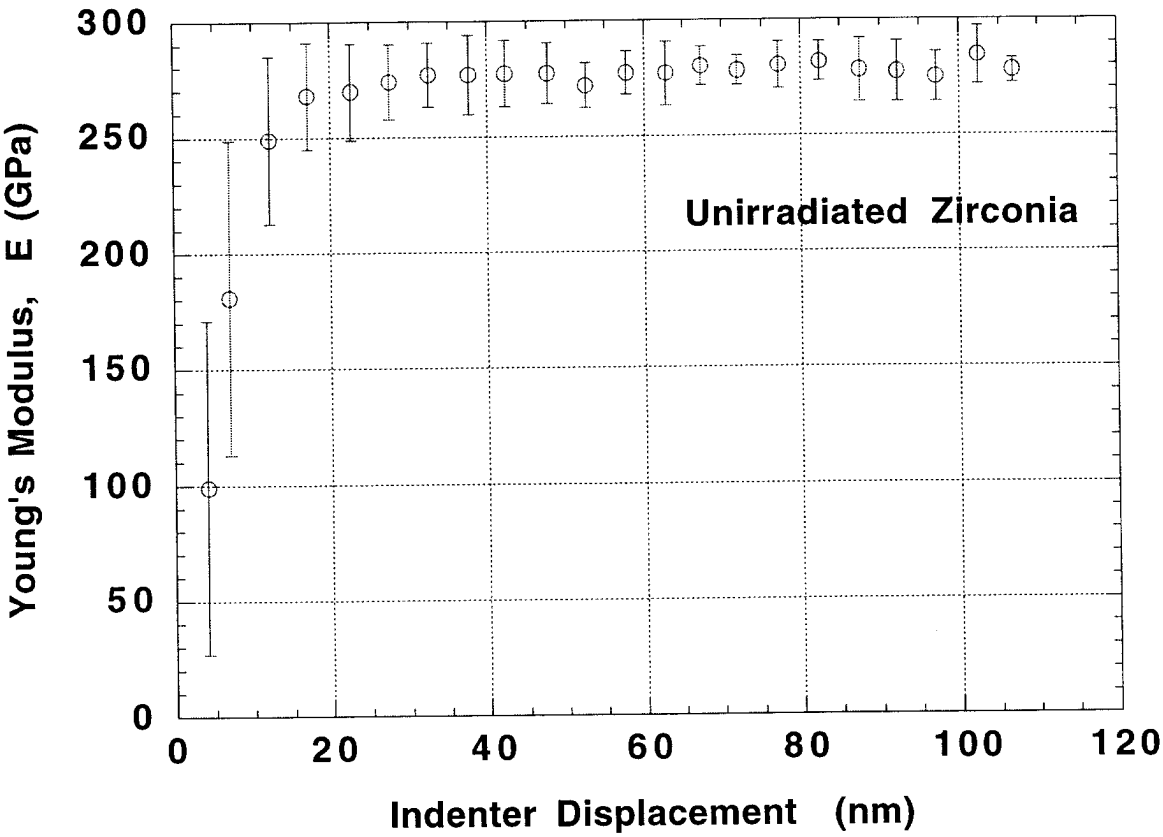
Young's Modulus, E (GPa)
300
250
200
150
100
50
0
0
20
40
60
80
100
120
Indenter Displacement (nm)
Unirradiated Zirconia

Figure 2b

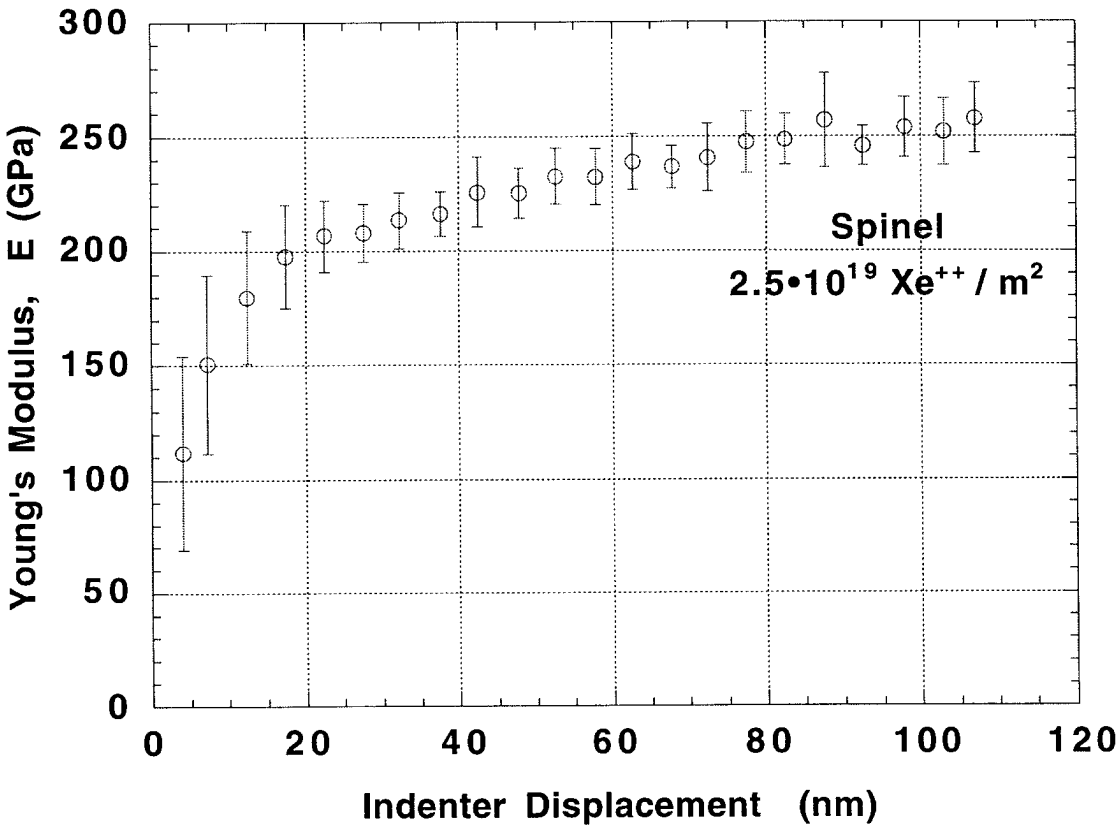
300
250
200
150
100
50
0
Young's Modulus, E (GPa)
0
20
40
60
80
100
120
Indenter Displacement (nm)
Spinel
2.5•10^19 Xe^++ / m^2

Figure 3a

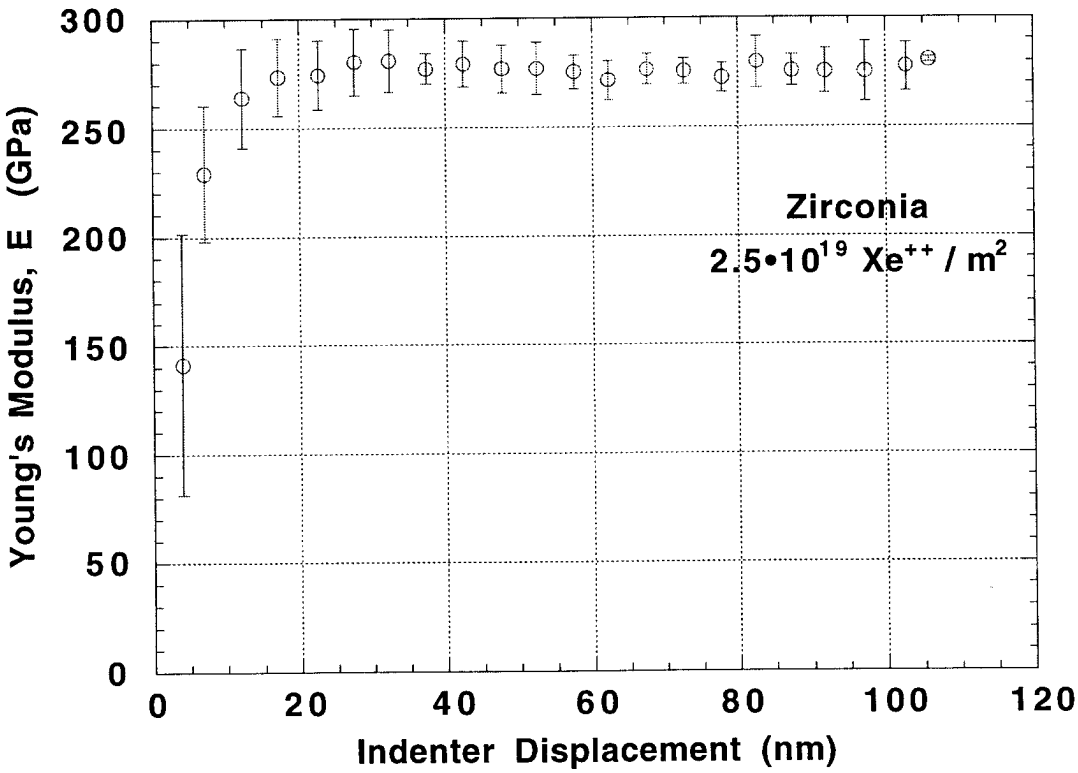
Young's Modulus, E (GPa)
300
250
200
150
100
50
0
0
20
40
60
80
100
120
Indenter Displacement (nm)
Zirconia
2.5•10^19 Xe^++ / m^2

Figure 3b

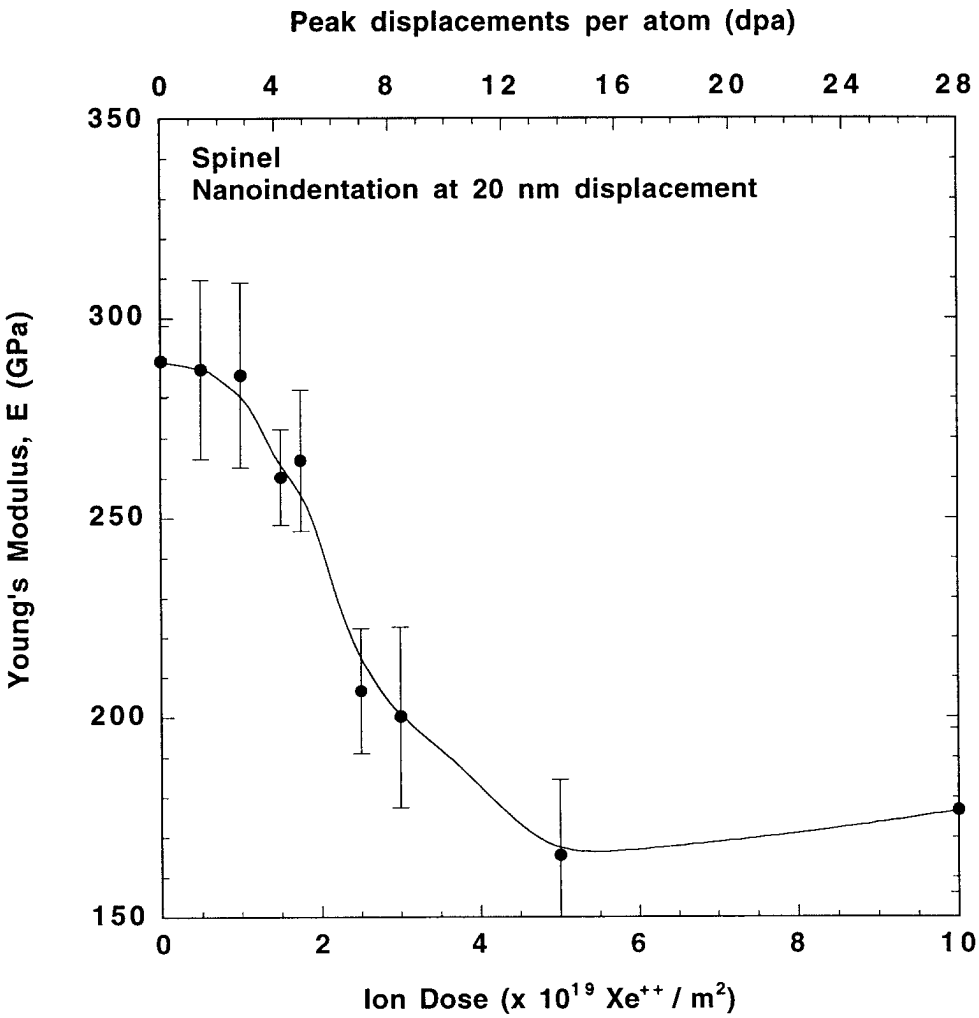
Peak displacements per atom (dpa)
0
4
8
12
16
20
24
28
350
300
250
200
150
Spinel
Nanoindentation at 20 nm displacement
Young's Modulus, E (GPa)
0
2
4
6
8
10
Ion Dose (x 10^19 Xe++ / m^2)

Figure 4a

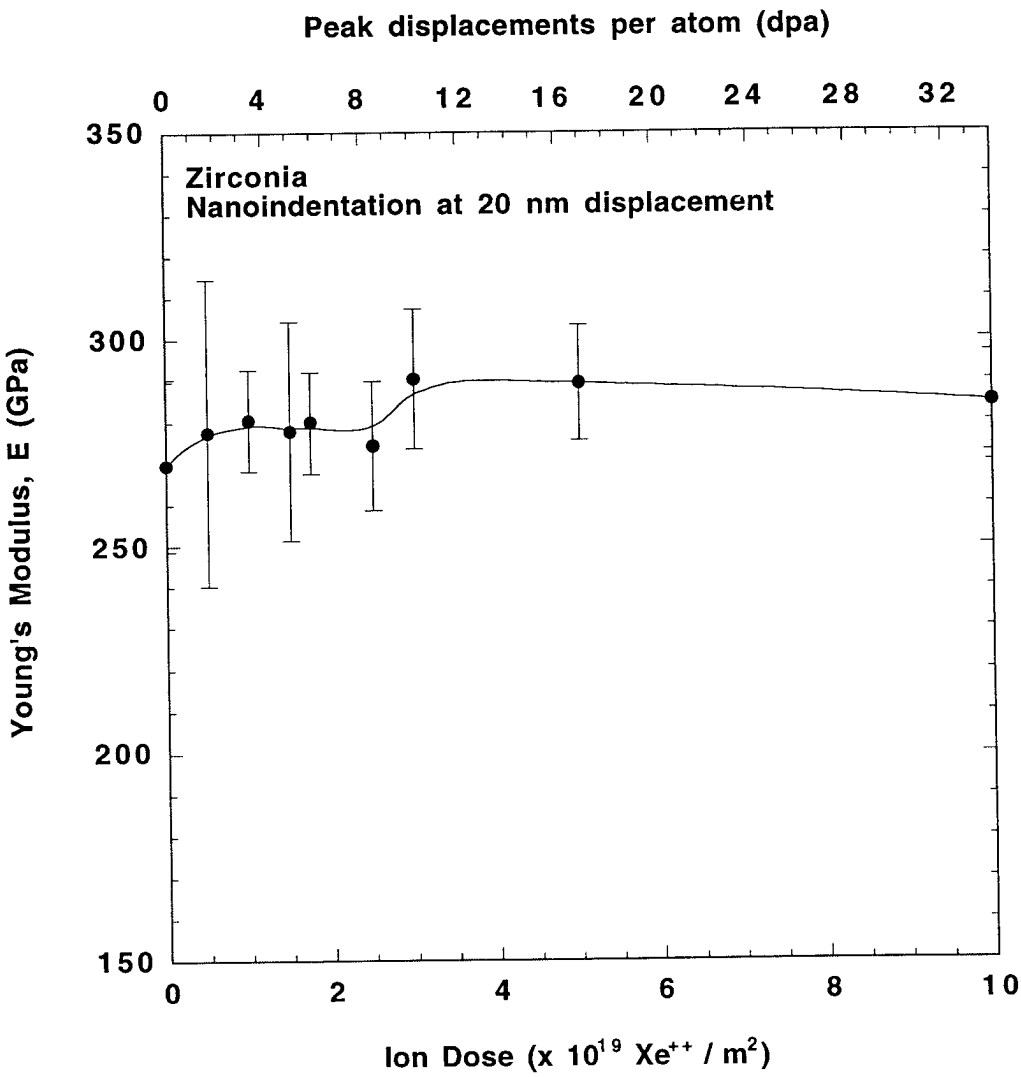
Peak displacements per atom (dpa)
0
4
8
12
16
20
24
28
32
350
300
250
200
150
Zirconia
Nanoindentation at 20 nm displacement
Young's Modulus, E (GPa)
0
2
4
6
8
10
Ion Dose (x 10^19 Xe++ / m^2)

Figure 4b

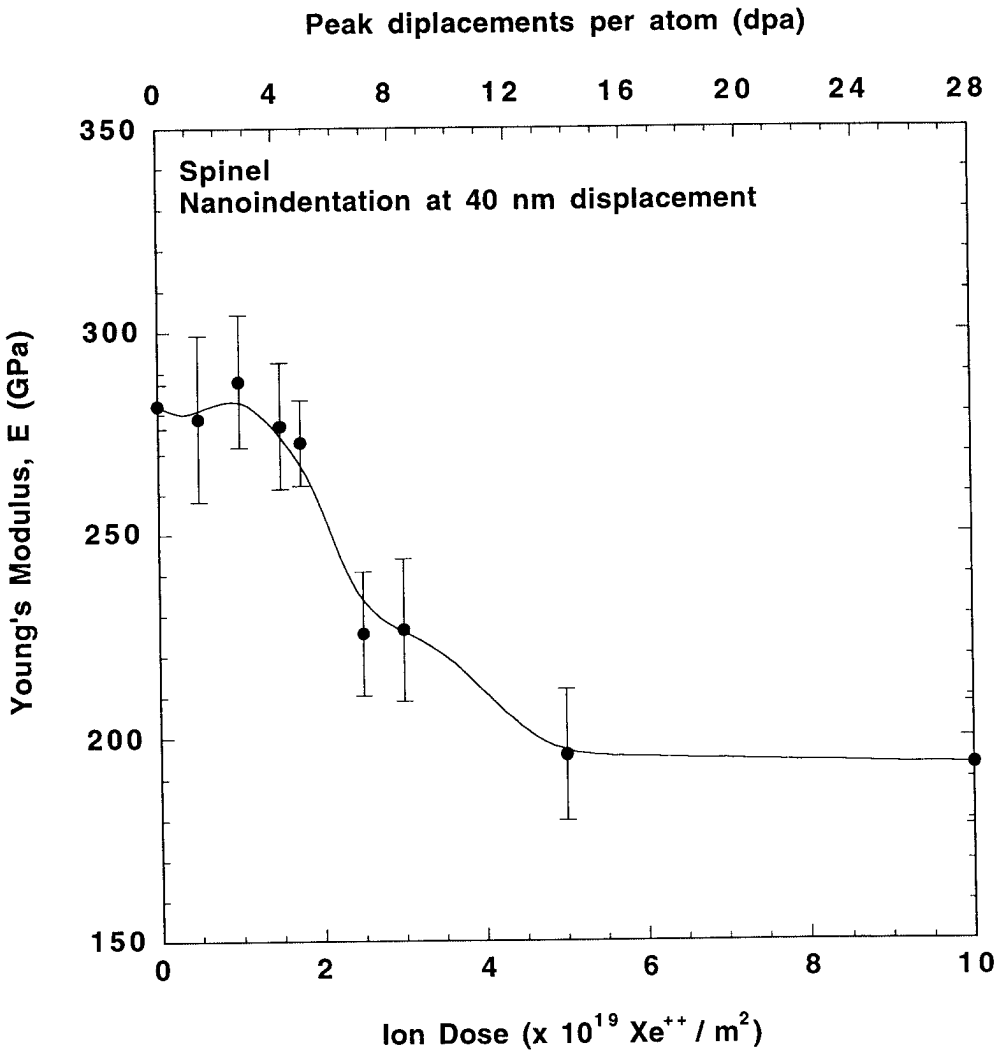
Peak diplacements per atom (dpa)
0
4
8
12
16
20
24
28
350
300
250
200
150
Spinel
Nanoindentation at 40 nm displacement
Young's Modulus, E (GPa)
0
2
4
6
8
10
Ion Dose (x 10^19 Xe^++ / m^2)

Figure 5a

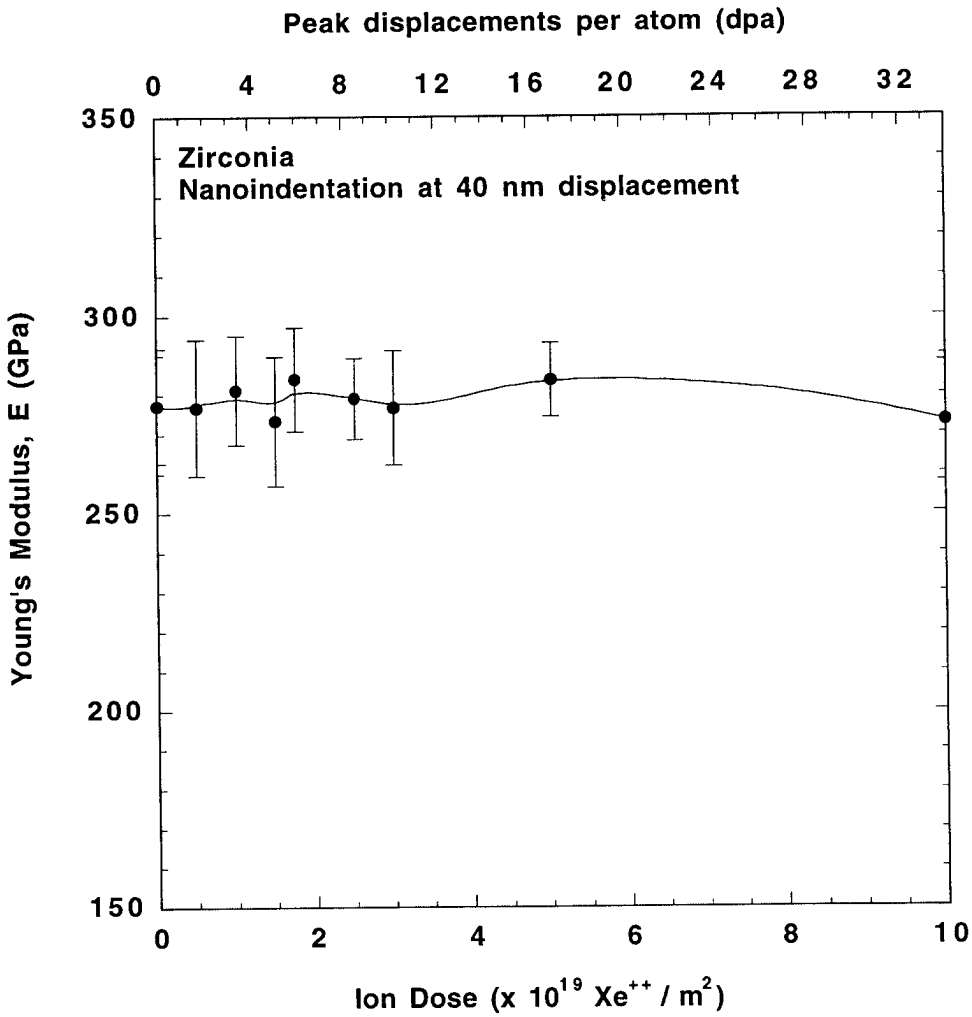
Peak displacements per atom (dpa)
0
4
8
12
16
20
24
28
32
350
300
250
200
150
Zirconia
Nanoindentation at 40 nm displacement
Young's Modulus, E (GPa)
0
2
4
6
8
10
Ion Dose (x 10^19 Xe^++ / m^2)

Figure 5b

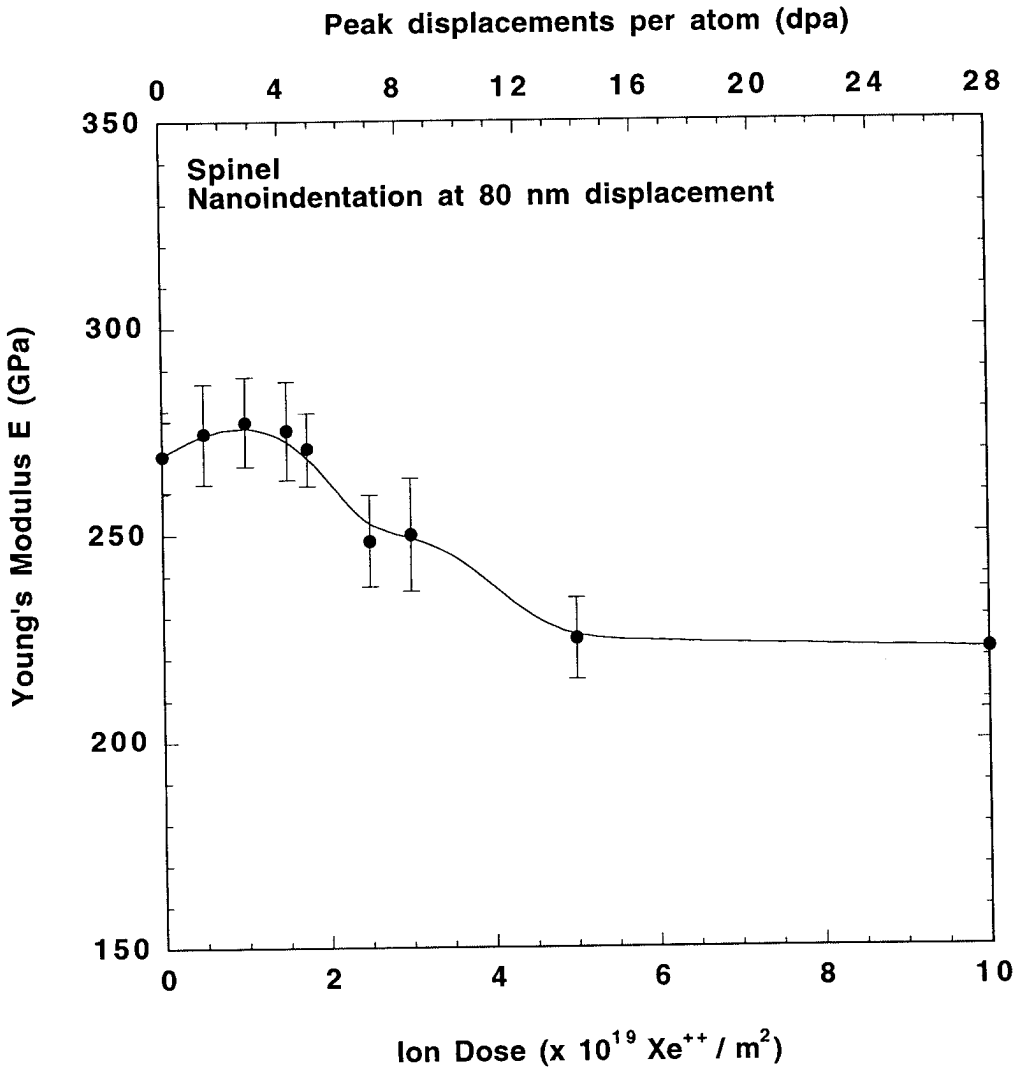
Peak displacements per atom (dpa)
0
4
8
12
16
20
24
28
350
300
250
200
150
Spinel
Nanoindentation at 80 nm displacement
Young's Modulus E (GPa)
0
2
4
6
8
10
Ion Dose (x 10^19 Xe++ / m^2)

Figure 6a

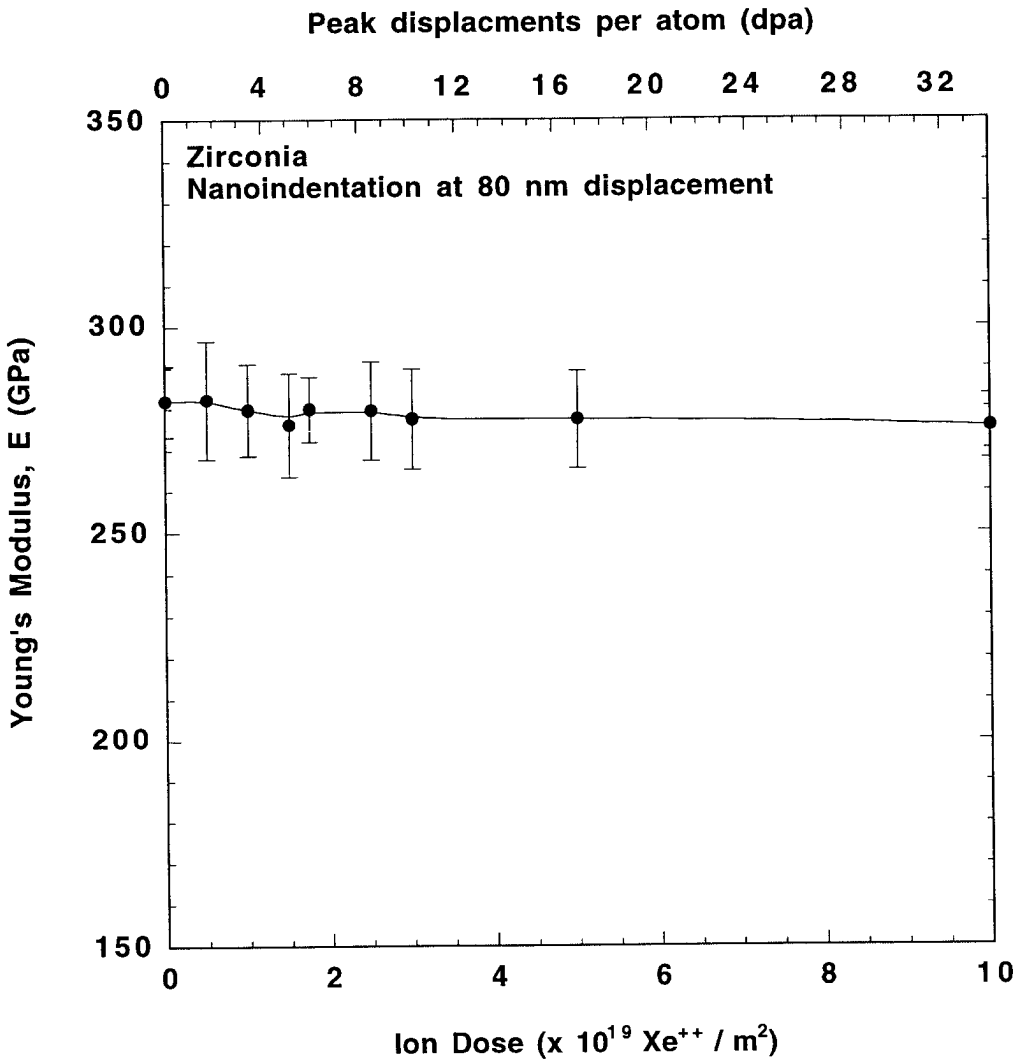
Peak displacments per atom (dpa)
0
4
8
12
16
20
24
28
32
350
300
250
200
150
Zirconia
Nanoindentation at 80 nm displacement
Young's Modulus, E (GPa)
0
2
4
6
8
10
Ion Dose (x 10^19 Xe++ / m^2)

Figure 6b

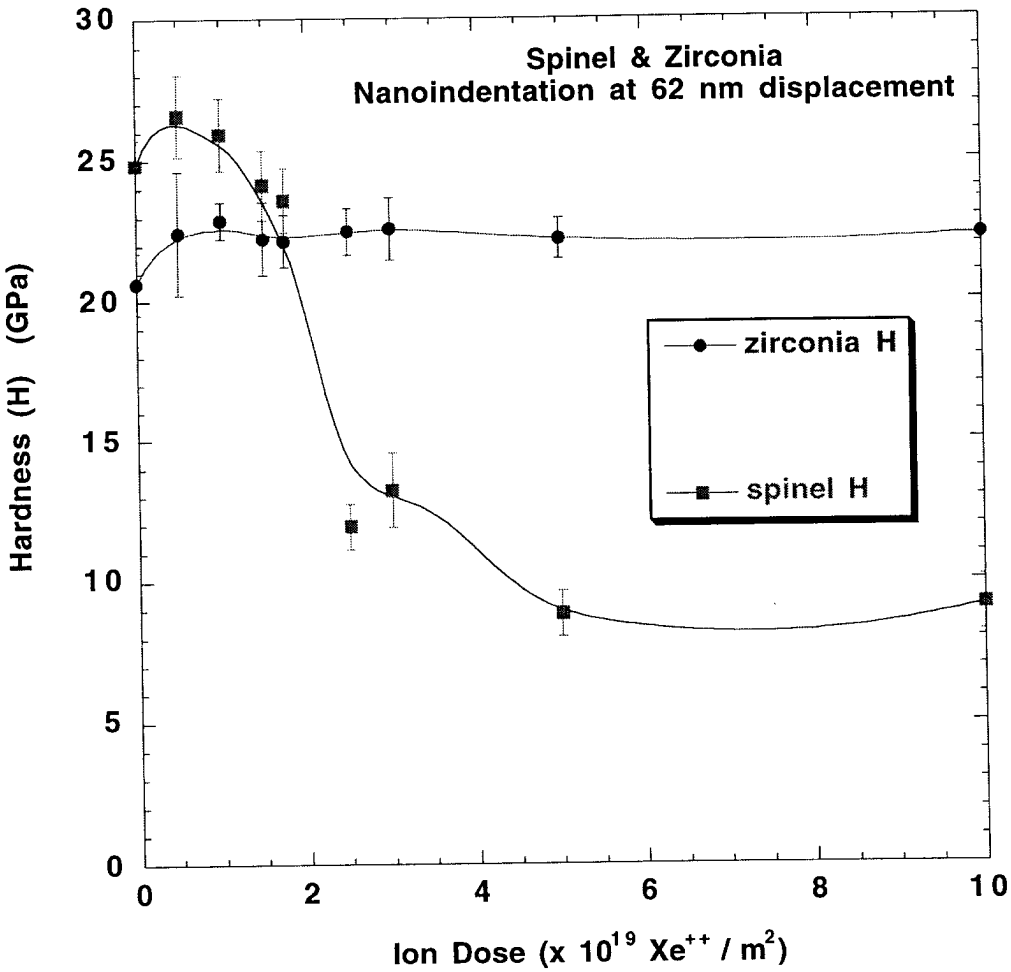
Spinel & Zirconia
Nanoindentation at 62 nm displacement
Hardness (H) (GPa)
Ion Dose (x 10^19 Xe++ / m^2)
zirconia H
spinel H
0
5
10
15
20
25
30
0
2
4
6
8
10

Figure 7

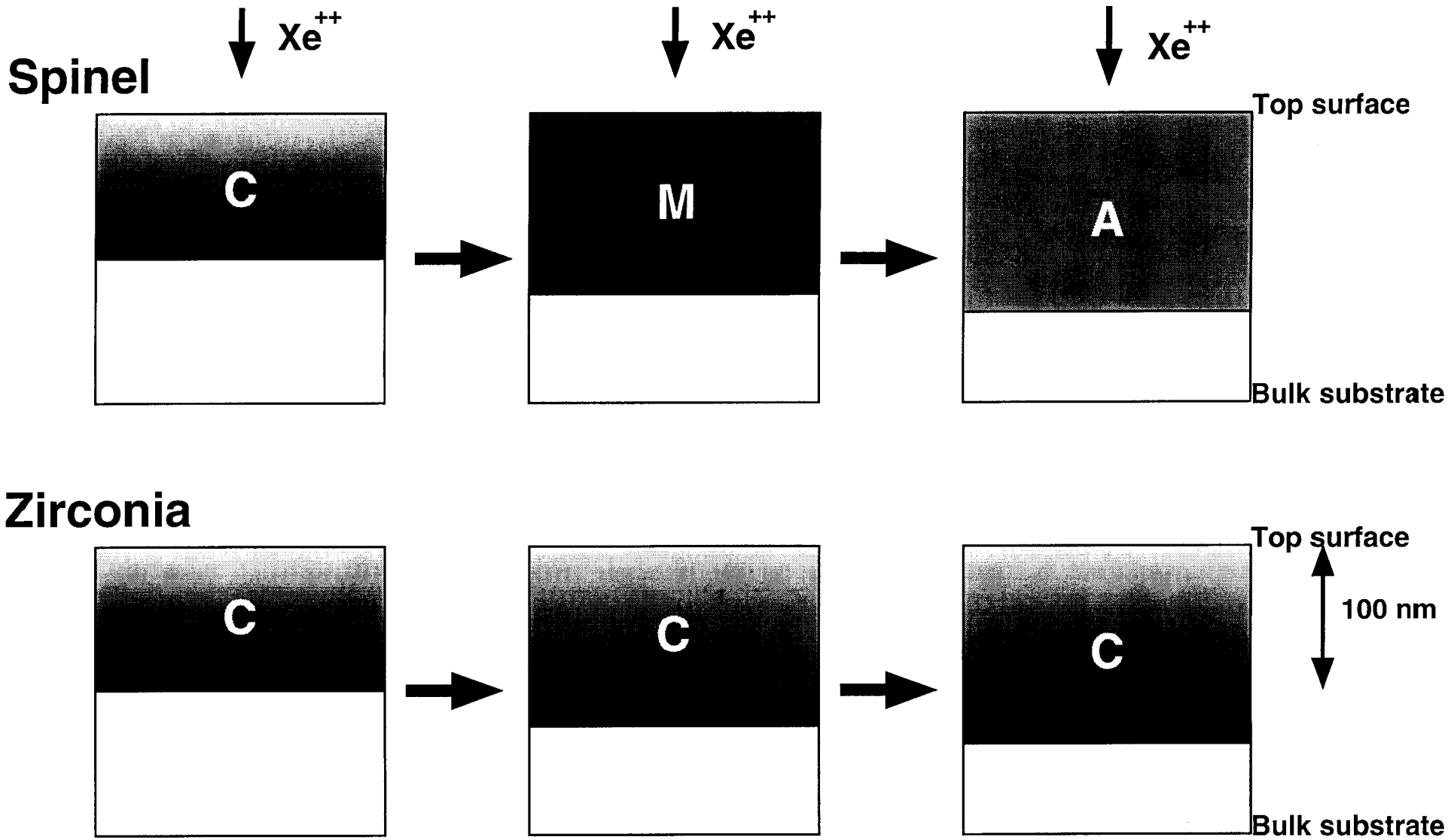
Spinel
Xe++
Xe++
Xe++
C
M
A
Top surface
Bulk substrate
Zirconia
C
C
C
Top surface
100 nm
Bulk substrate
5•10^18 Xe++/m^2
1.5•10^19 Xe++ /m^2
1•10^20 Xe++/m^2
peak damage
1.4 dpa, spinel
1.7 dpa, zirconia
peak damage
4.2 dpa, spinel
5.1 dpa, zirconia
peak damage
28 dpa, spinel
34 dpa, zirconia

Figure 8

Report Number (14) LA-UR--97-4004
CONF-9705230--

Publ. Date (11) 199712
Sponsor Code (18) DOE/MA, XF
JC Category (19) UC-904, DOE/ER

DOE